Supplementary Information

Myeloid Cell Replacement Induces Intercellular Mitochondrial Transfer and Restores Metabolism in a Mouse Model of Mitochondrial disease

Author list

Hyunmin Cho[1], Ruhi Sayana[1], Abhishek Koladiya[2], Pasqualina Colella[1], Sangkyun Cho[3], James W.S. Jahng[3], Juan Jose Vasquez[1], Jessica Arozqueta Basurto[1], Joseph C Wu[3,4], Natalia Gomez-Ospina[1,5*]

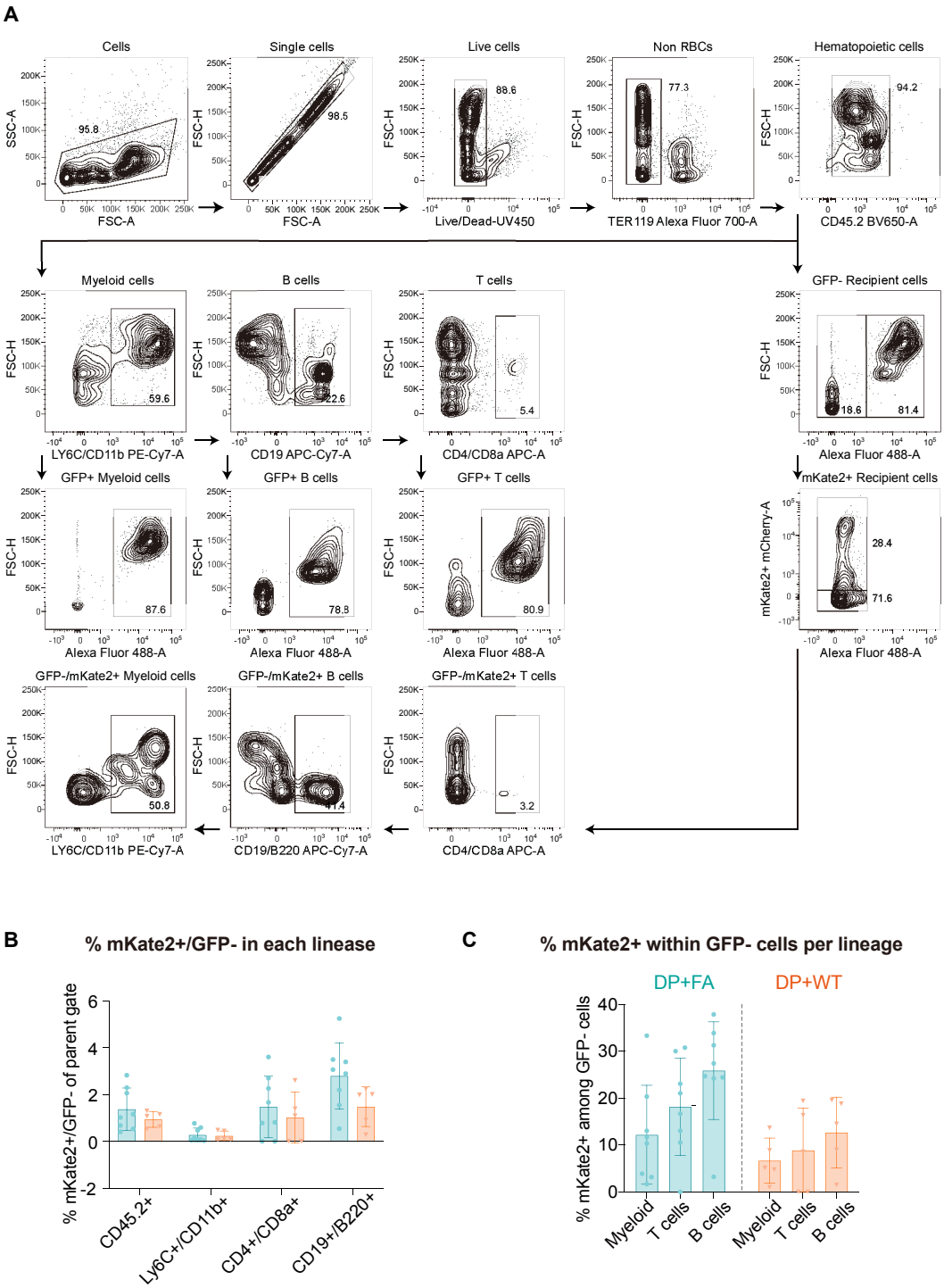

Supplementary Fig. 1. Gating strategy for analyzing hematopoietic lineages, donor chimerism, and mitochondrial transfer in hematopoietic tissues. (A) Representative gating strategy for analyzing cells isolated from hematopoietic tissues including bone marrow, spleen, and peripheral blood. The representative flow plots come from a bone marrow DP+FA sample and depict the gating strategy used to calculate the percentage of marker-positive cells among CD45+ cells, the percentage of donor-derived GFP+ cells post-transplant, the proportion of mKate2+/GFP- cells indicating mitochondrial transfer, and the proportion of different markers within the mKate2+/GFP- population. The analysis was conducted 5 months after transplantation. Flow plots are representative of biologically independent mice with similar results. **(B)** Quantification of mKate2$^+$/GFP$^-$ cells across hematopoietic lineages in bone marrow. Percentage of mKate2$^+$/GFP$^-$ cells within the parent lineage gate (CD45.2$^+$, Ly6C$^+$/CD11b$^+$ for myeloid cells, CD4$^+$/CD8a$^+$ for T cells, and CD19$^+$/B220$^+$ for B cells) in DP+FA and DP+WT conditions. **(C)** Percentage of mKate2$^+$ cells within the GFP$^-$ compartment for each lineage. Data are shown as individual mice with mean ± SD.Each symbol represents one biologically independent mouse [*n* = 8 DP+FA and 5 DP+WT]. Source data are provided as a Source Data file.

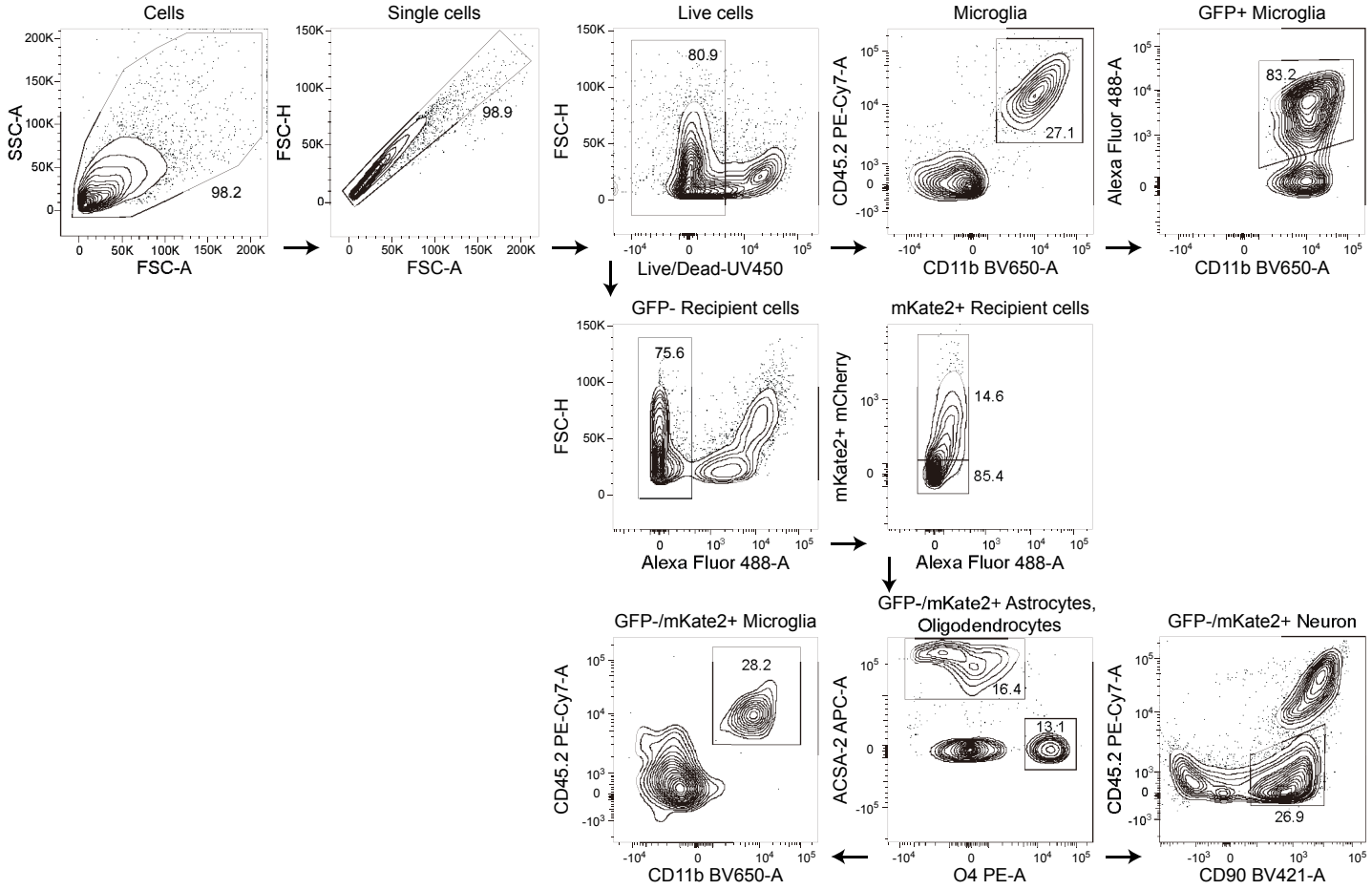

Supplementary Figure 2. Gating strategy for analyzing donor chimerism and mitochondrial transfer in the brain. Representative gating strategy for flow cytometric analysis of cells isolated from the brains of YG8-800 FA mice transplanted with bone marrow cells from GFP/mKate2+ double-positive mice. The plots illustrate the gating strategy used to quantify the percentage of transplant-derived GFP+ cells and to observe mitochondrial movement by measuring mKate2. Gating strategies for quantifying the major cell types present in the brain—neurons, astrocytes, oligodendrocytes, and microglia—are also included. The analysis was conducted five months after transplantation. Flow plots are representative of biologically independent mice with similar results. Flow plots are representative of biologically independent mice with similar results.

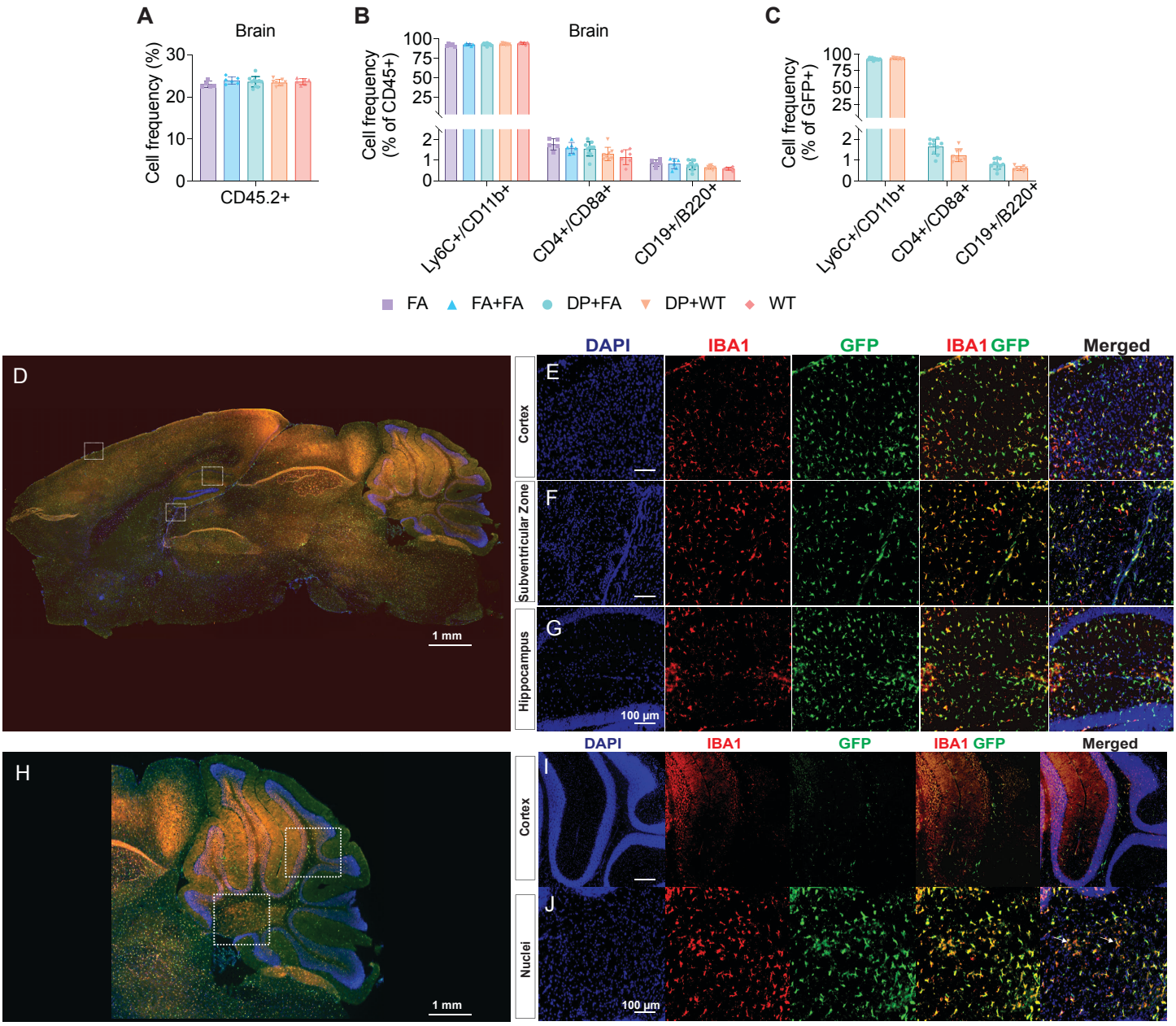

Supplementary Figure 3. Immune cell composition in the brain following microglia replacement. (A–C) Flow cytometric analysis of hematopoietic (CD45+) cells as a fraction of live cells in the brain five months post-transplantation across experimental groups (FA, FA+FA, DP+FA, DP+WT, and WT). **(A)** Frequency of total CD45+ cells after isolation. **(B)** Proportional distribution of CD45+ subsets expressing CD11b/Ly6C (myeloid), CD19/B220 (B cell), and CD4/CD8a (T cell) markers. **(C)** Marker distribution among GFP+ cells. Data are presented as mean ± SEM. Each symbol represents one biologically independent mouse [n = 5 per group]. Comparisons were done using one-way ANOVA with Tukey's multiple comparison test; no significant found, exact p-values are provided in the Source Data file. Source data are provided as a Source Data file. **(D–J)** Engraftment of GFP+/IBA1+ donor-derived microglia-like cells throughout the brain following microglia replacement. **(D)** Representative sagittal section of an engrafted DP+WT mouse brain. Higher-magnification images demonstrate colocalization of GFP (green) and IBA1 (red) in the **(E)** cortex, **(F)** subventricular zone, and **(G)** hippocampus, confirming near-complete overlap of GFP+ and IBA1+ signals. **(H–J)** Analysis of the cerebellum showing **(H)** a representative sagittal section and widespread engraftment of GFP+/IBA1+ cells in the **(I)** cerebellar cortex and **(J)** deep cerebellar nuclei. Nuclei are counterstained with DAPI (blue). Scale bars: 1 mm (D, H); 100 µm (E–G, I–J). Images are representative of [*n* = 5] mice per group with similar results. Scale bars: 1 mm (D, H); 100 µm (E–G, I–J).

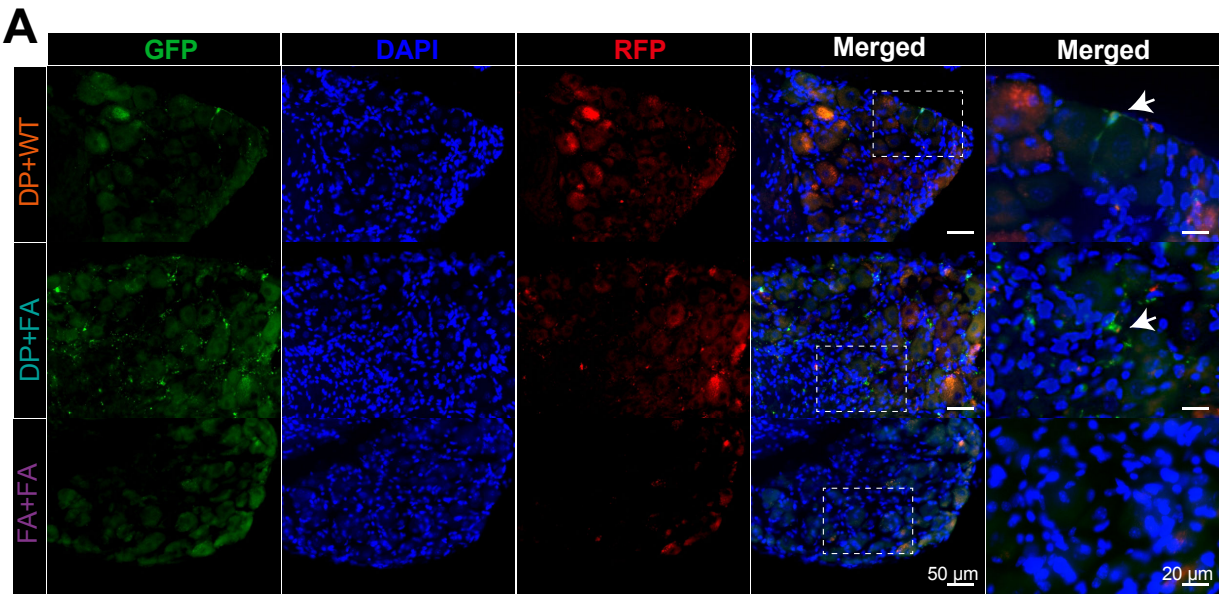

Supplementary Figure 4. Analysis of bone marrow–derived cell infiltration in dorsal root ganglia. Representative epifluorescence images of DRG sections from wild-type recipients transplanted with double-positive cells (DP→WT), FA recipients transplanted with double-positive cells (DP→FA), and FA recipients transplanted with FA cells (FA→FA). Sections were imaged for GFP (green) to identify donor-derived cells, RFP (red) to identify mKate2, and DAPI (blue) for nuclei. Images are representative of [*n* = 5] mice per group with similar results. Scale bars: 1 mm (D, H); 100 µm (E–G, I–J). Scale bars: 50 µm (left panels) and 20 µm (magnified insets).

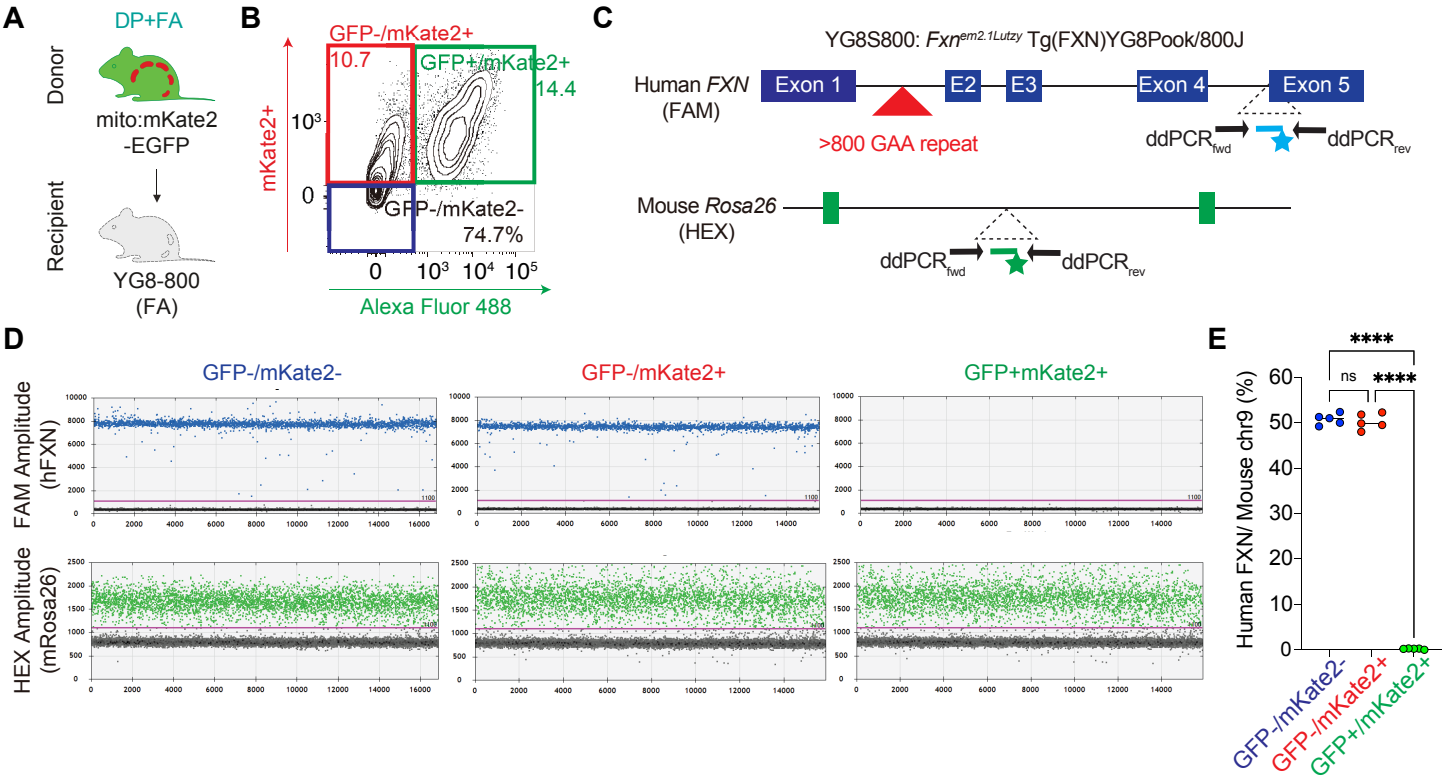

Supplementary Fig. 5. Droplet digital PCR assay to establish identity of GFP-/mKate2+ cells. (A–B) Schematic overview and FACS gating strategy used to isolate GFP-/mKate2+, GFP-/mKate2+, and GFP-/mKate2+ cells from the brain of the DP+FA group for ddPCR analysis. **(C)** Diagram of the ddPCR design. A FAM-labeled probe (blue star) targeting the region flanking exon 5 of the integrated human *FXN* YAC transgene (hemizygous) was used to identify human FXN sequences. A HEX-labeled probe (green star) targeting the murine *Rosa26* locus served as the reference assay. **(D)** Representative one-dimensional ddPCR plots showing fluorescence signal distributions for each brain cell population. Both GFP-/mKate2- and GFP-/mKate2+ fractions amplified the human *FXN* transgene, confirming their FA mouse origin, whereas GFP+/mKate2+ donor cells lacked *FXN* amplification. Blue droplets indicate FAM+ (hFXN), and green droplets indicate HEX+ (mRosa26) events. **(E)** Relative allele abundance, expressed as the ratio of hFXN to mRosa26 (copies/µL), for GFP-/mKate2- (blue, n = 5), GFP-/mKate2+ (red, n = 5), and GFP+/mKate2+ (green, n = 5) populations. Data are presented as mean ± SD. Each symbol represents one biologically independent mouse; statistical analysis was a two-sided one-way ANOVA with Tukey's multiple comparisons test, Significant differences are indicated by asterisks (****p < 0.0001) and exact p-values are provided in the Source Data file. Source data are provided as a Source Data file.

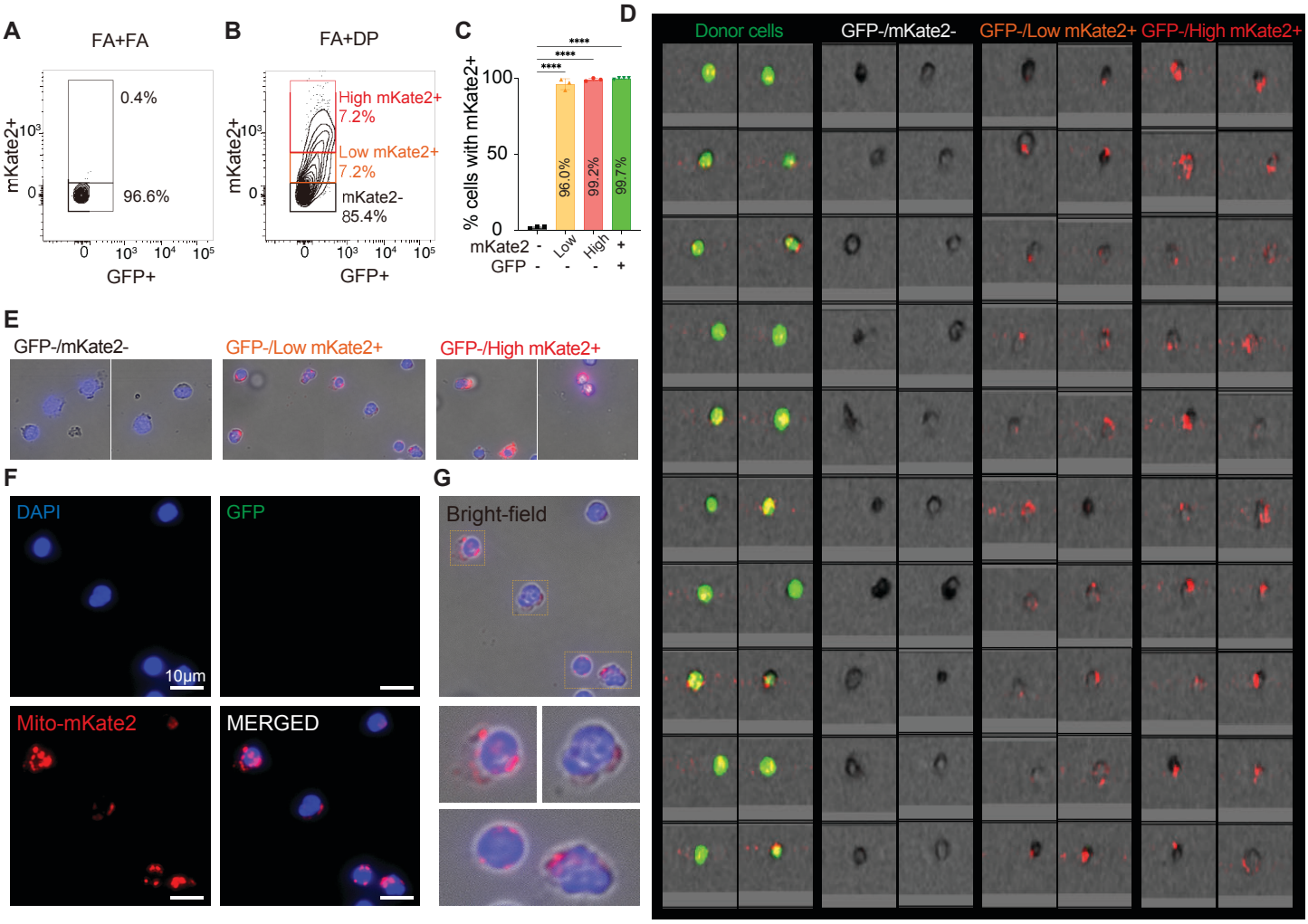

Supplementary Fig. 6. Flow cytometry and imaging analysis of GFP-/mKate2+ acceptor cells following transplantation. (A-B) Representative FACS plots showing the proportion of mKate2+ and GFP+ cells in dissociated cell populations from brains from FA mice transplanted with FA cells **(A)** or DP cells **(B)** showing gating strategy. Cells were analyzed in BD FACSDiscover™ S8 Cell Sorter with BD CellView™ Image Technology which combines spectral flow cytometry with real-time imaging. **(C)** Quantification of the fraction of cells with mKate2+ puncta among GFP- (acceptor) or GFP+ (donor) cells in three independent mice. Four hundred cells analyzed per mouse. Data presented as mean ± SD. Statistical analysis for C, was a two-sided one-way ANOVA with Tukey's multiple comparisons test. Significant differences are indicated by asterisks (****p < 0.0001). Exact p-values are provided in the Source Data file. Source data are provided as a Source Data file. **(D)** Representative BD CellView™ Image images of GFP-/mKate2-, GFP+/mKate2+ donor, and GFP-/mKate2+ acceptor subsets (Low and High mKate2+). **(E)** Bright-field and fluorescence overlay images of sorted GFP-/mKate2-, GFP-/Low mKate2+, and GFP-/High mKate2+ cells. **(F)** High-magnification images showing DAPI (nuclei, blue), GFP (green), and Mito-mKate2 (red) channels with merged view. Scale bar, 10 µm. **(G)** Bright-field merged images of representative GFP-/mKate2+ acceptor cells illustrating cytoplasmic mKate2 puncta. Images in (**E–G**) are representative of n = 3 mice with similar results.

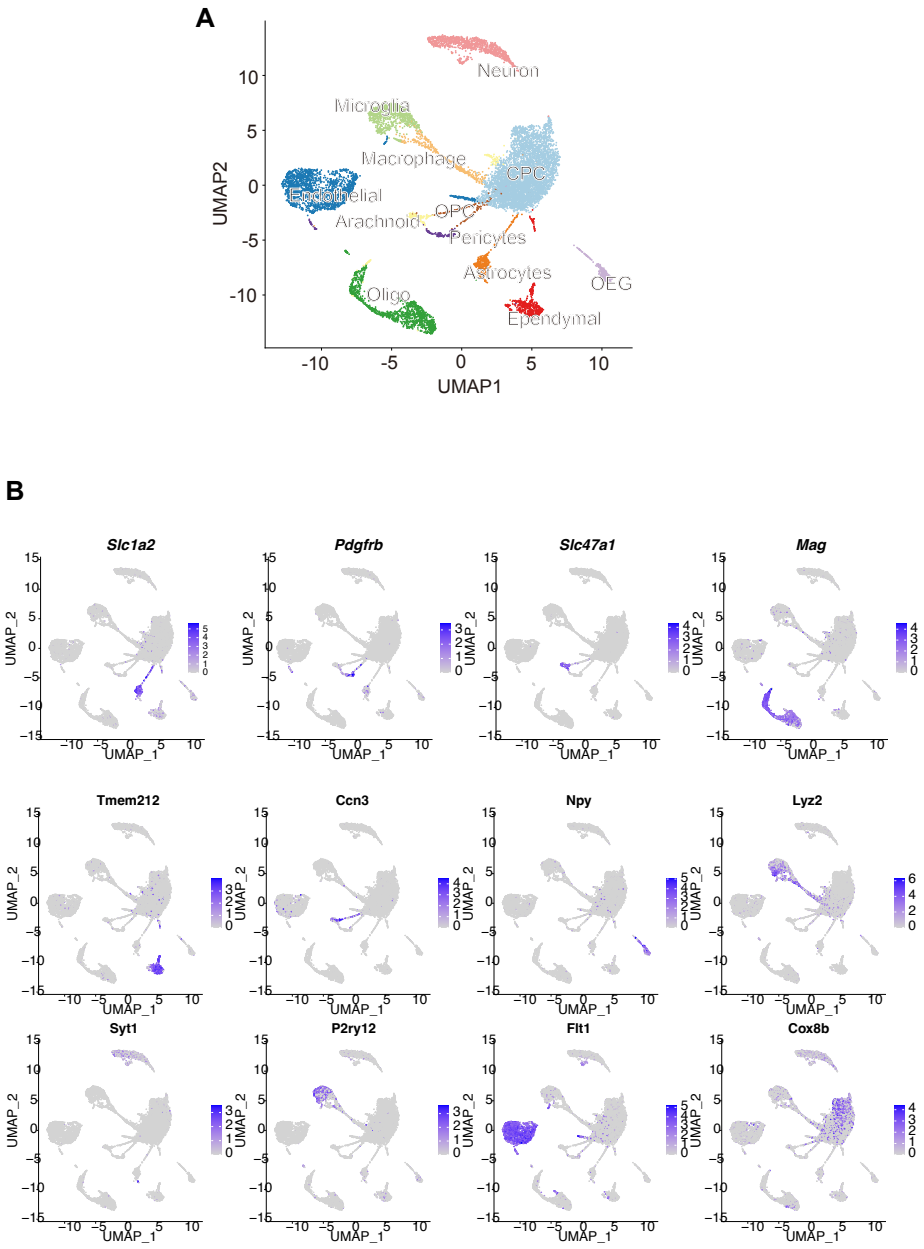

Supplementary Figure 7. UMAP representations of representative marker gene expression for the twelve CNS cell types. UMAP plots of single-cell RNA-sequencing data (12,347 GFP− recipient brain cells pooled from three biologically independent DP+FA mice) showing expression of a representative marker gene per cell type. Astrocytes: *Slc1a2*, Pericytes: *Pdgfrb*, ABC: *Slc4a71*, Oligodendrocytes: *Mag*, Ependymal Cells: *Tmem212*, OPC: *Ccn3*, OEG: *Npy,* Macrophages: *Lyz2*, Neurons: *Syt1*, Microglia: *P2ry12*, Endothelial cells: *Flt1*, CPCs: *Cox8b.* The color scale indicates normalized expression level (low to high).

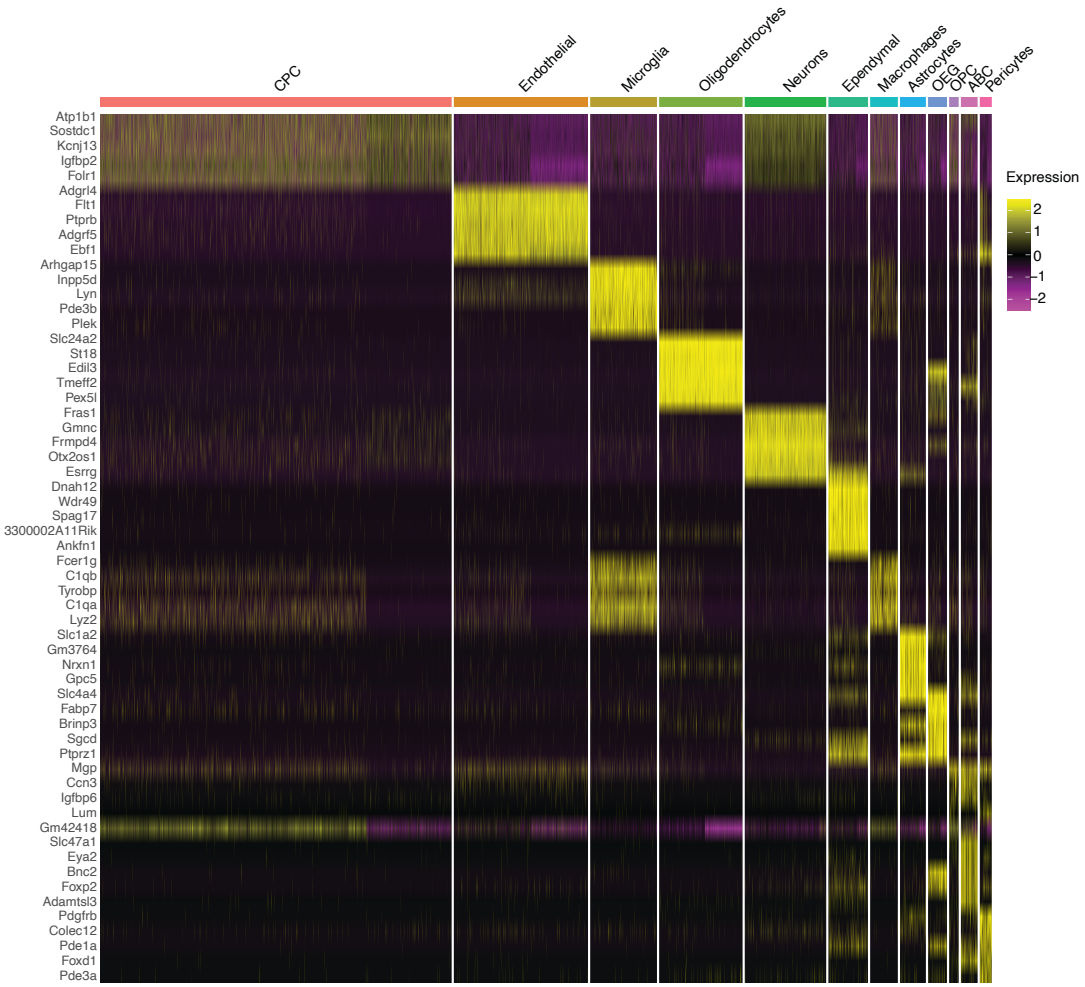

Supplementary Fig. 8. Heatmap of gene expression across CNS cell types following mitochondrial uptake. Data are from single-cell RNA sequencing of 12,347 GFP− recipient cells pooled from three biologically independent DP+FA mice. The heatmap shows the expression patterns of selected genes across various CNS cell types after mitochondrial acquisition, including choroid plexus cells (CPCs), endothelial cells, microglia, macrophages, oligodendrocytes, neurons, ependymal cells, astrocytes, olfactory ensheathing glia (OEG), oligodendrocyte precursor cells (OPC), arachnoid barrier cells (ABC), and pericytes. Each row represents a gene, and each column represents a different cell type. The color scale indicates relative expression levels, with yellow indicating high expression, purple indicating low expression, and black representing intermediate expression levels. Distinct clusters of gene expression patterns are observed, highlighting cell type-specific transcriptional responses.

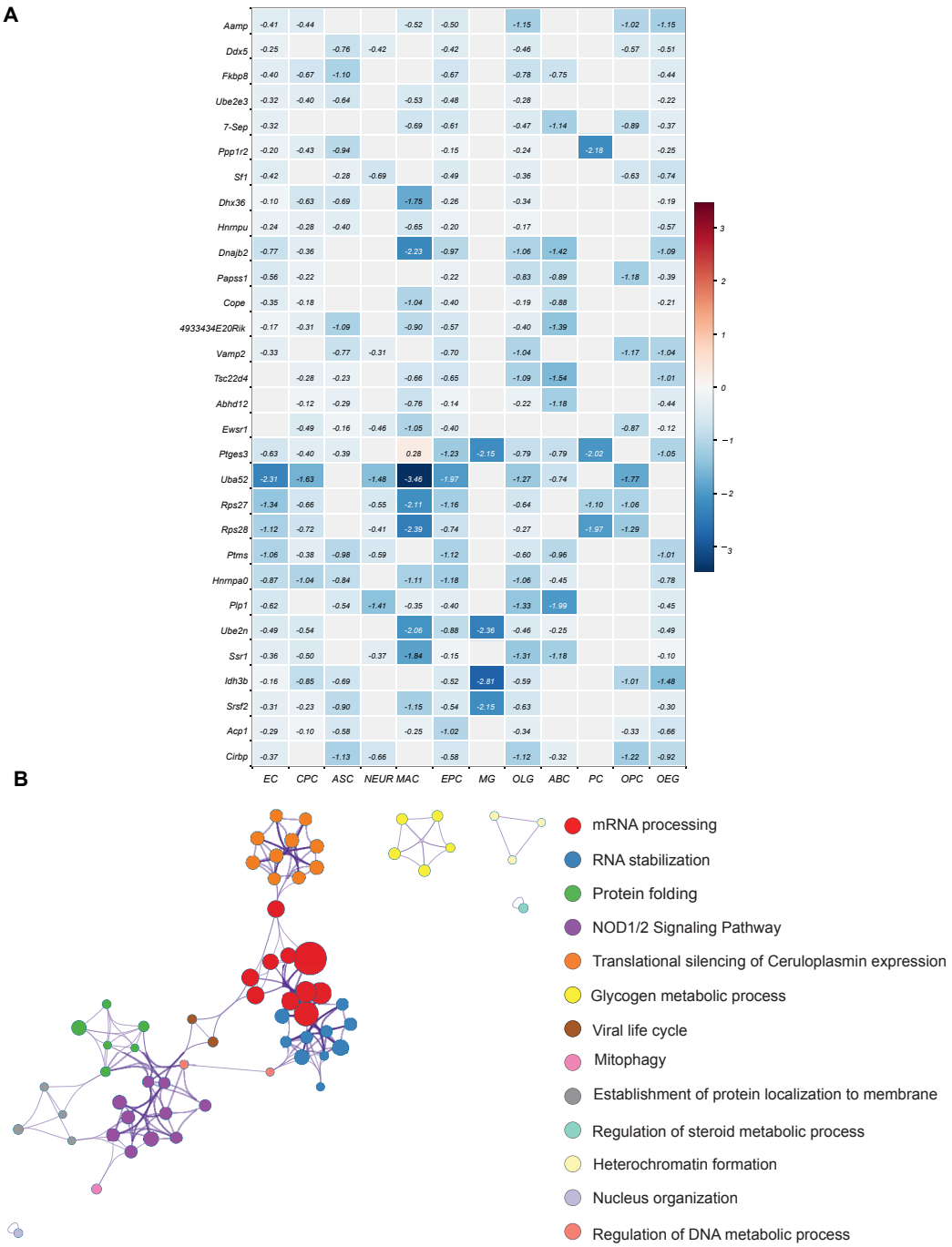

Supplementary Fig. 9. Analysis of downregulated genes and associated pathways in mKate2+ cells across CNS cell types. (A) Heatmap showing the expression levels of commonly downregulated genes in various CNS cell types in mKate2+ cells, including endothelial cells (EC), choroid plexus epithelial cells (CPC), astrocytes (ASC), neurons (NEU), macrophages (MAC), ependymal cells (EPC), microglia (MG), oligodendrocytes (OLG), arachnoid barrier cells (ABC), oligodendrocyte precursor cells (OPC), pericytes (PC), and olfactory ensheathing glia (OEG). The color scale represents relative expression changes, with shades of blue indicating downregulation, red indicating upregulation, and gray representing non-detected data. Differentially expressed genes were identified with the two-sided MAST test with Benjamini–Hochberg FDR correction (adjusted $p < 0.05$, fold change > 20%). Source data are provided as a Source Data file. **(B)** Network map illustrating enriched biological processes and pathways associated with the commonly downregulated genes across multiple cell types. Nodes represent individual pathways, colored according to functional categories, with node size reflecting the significance of enrichment. The network map includes pathways related to mRNA processing (red), RNA stabilization (blue), protein folding (green), NOD1/2 signaling (dark purple), translational silencing of ceruloplasmin expression (orange), glycogen metabolic processes (yellow), viral life cycle (dark brown), mitophagy (pink), establishment of protein localization to membranes (gray), regulation of steroid metabolic processes (teal), heterochromatin formation (light yellow), nucleus organization (light purple), and regulation of DNA metabolic processes (coral). Enrichment was assessed by over-representation analysis with Benjamini–Hochberg correction. Data are from single-cell RNA sequencing of 12,347 GFP– recipient cells (3,196 mKate2– and 9,151 mKate2+) pooled from three biologically independent DP+FA mice.

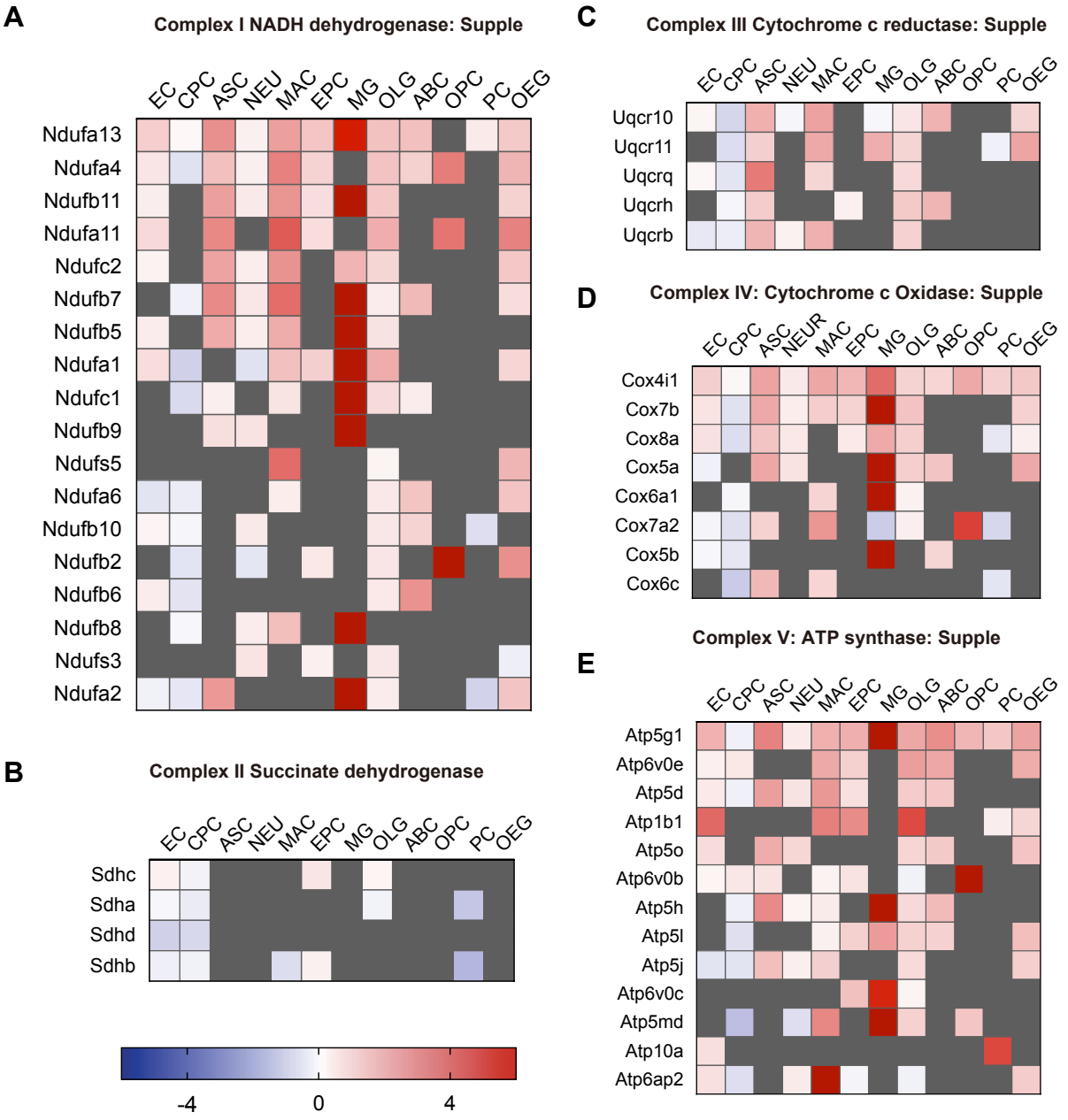

Supplementary Fig. 10. Changes in nuclear DNA-encoded mitochondrial subunit expression in YG8-800 mouse brain cells. (A-E) Heatmaps showing the log2 fold change (logFC) for Complex I NADH dehydrogenase **(A)**, Complex II Succinate dehydrogenase **(B)**, Complex III Coenzyme Q-cytochrome c reductase **(C)**, Complex IV Cytochrome c oxidase **(D)**, and Complex V ATP synthase **(E)**. Each row represents a gene, and each column represents a different CNS cell type. The color scale indicates fold change, with red shades representing over-expression, blue shades indicating under-expression, and dark gray representing non-significant data. Data are from single-cell RNA sequencing of 12,347 GFP− recipient cells pooled from three biologically independent DP+FA mice; differential expression was assessed with the two-sided MAST test with Benjamini–Hochberg FDR correction. Source data are provided as a Source Data file.

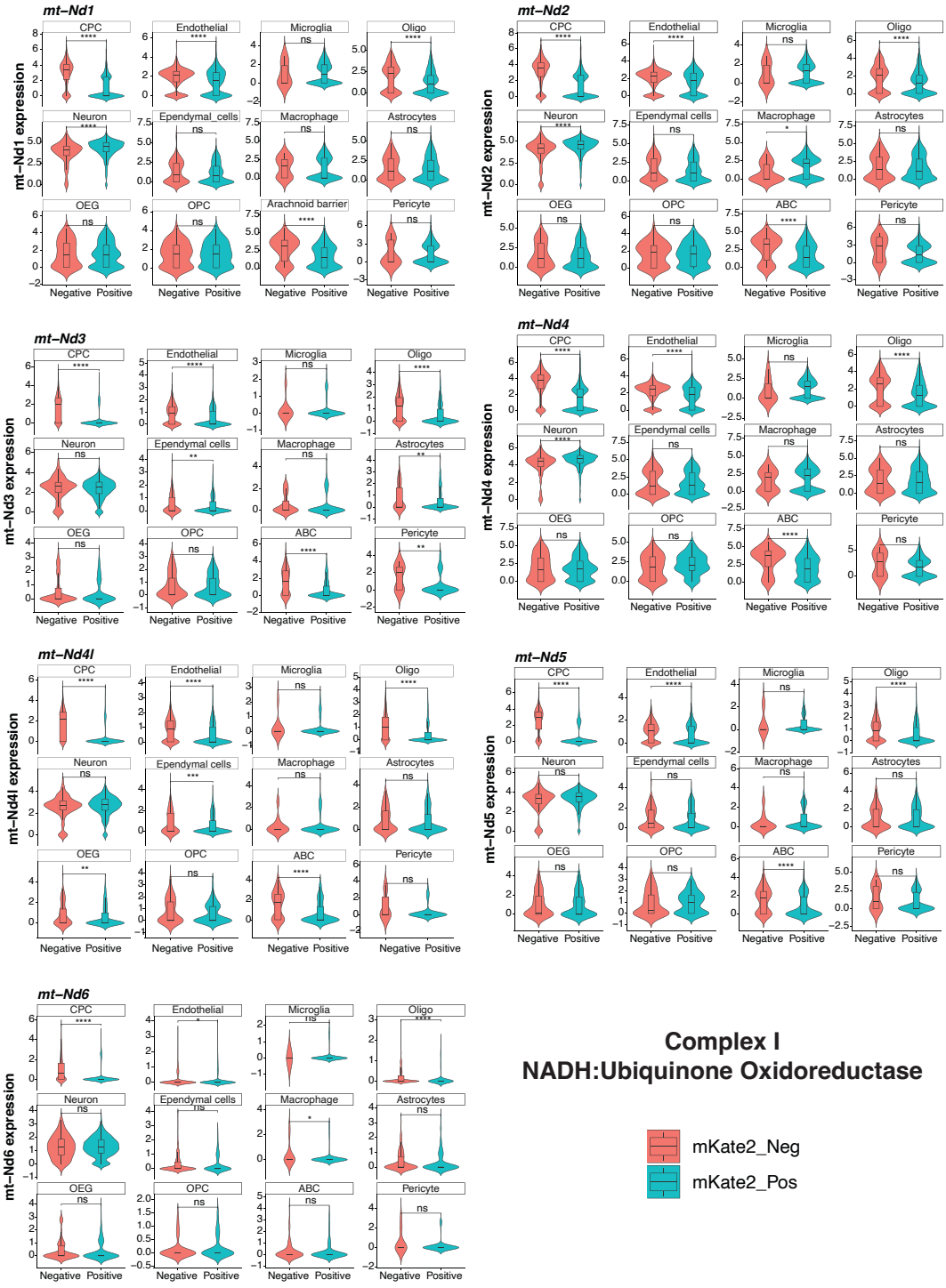

Supplementary Fig. 11. Differential expression of mitochondrial Complex I (NADH:Ubiquinone Oxidoreductase) mtDNA-encoded subunits across CNS cell types following mitochondrial uptake. Violin plots show the expression of each mitochondrial Complex I gene (mt-Nd1, mt-Nd2, mt-Nd3, mt-Nd4, mt-Nd4L, mt-Nd5, and mt-Nd6) in mKate2+ (teal) and mKate2- (red) cells across 12 CNS cell populations, including oligodendrocytes (Oligo), microglia, endothelial cells, choroid plexus cells (CPC), astrocytes, macrophages, ependymal cells, neurons, pericytes, arachnoid barrier cells (ABC), oligodendrocyte precursor cells (OPC), and olfactory ensheathing glia (OEG). Each panel displays the distribution and magnitude of expression differences for the indicated mtDNA gene. Pairwise comparisons between $mKate2^{+}$ and $mKate2^{-}$ cells were performed within each cell type using the two-sided Wilcoxon rank-sum text, with significance levels indicated as ns (not significant), *p < 0.05, **p < 0.01, ***p < 0.001, and ****p < 0.0001. Source data are provided as a Source Data file.

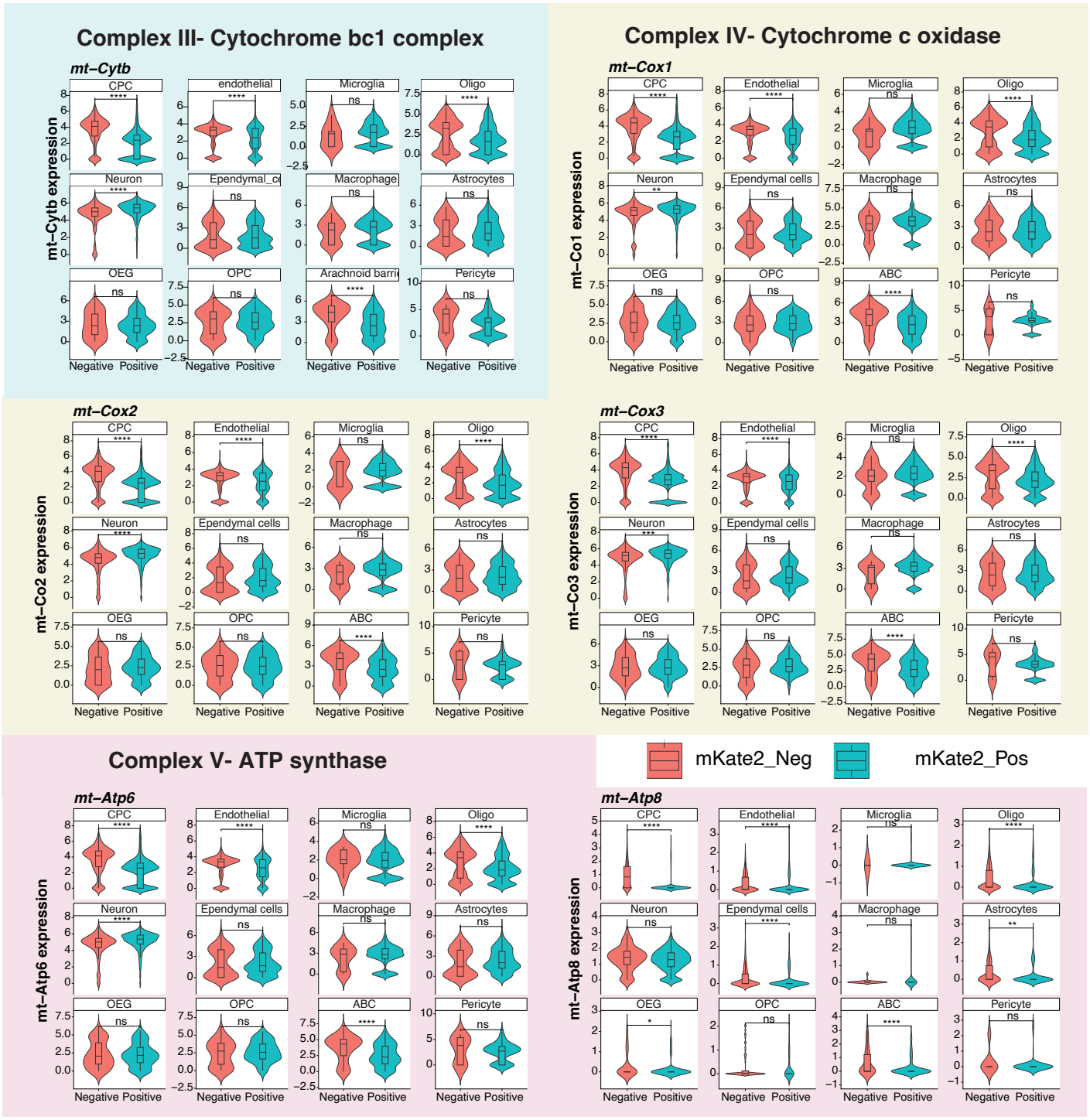

Supplementary Fig. 12. Differential expression of mitochondrial Complexes III, IV, and V mtDNA-encoded subunits across CNS cell types following mitochondrial uptake. Violin plots show the expression of mtDNA-encoded electron-transport-chain genes for Complex III (mt-Cytb), Complex IV (mt-Cox1, mt-Cox2, mt-Cox3), and Complex V (mt-Atp6, mt-Atp8) in mKate2+ (teal) and mKate2- (red) cells across 12 CNS cell types (oligodendrocytes (Oligo), microglia, endothelial cells, choroid plexus cells (CPC), astrocytes, macrophages, ependymal cells, neurons, pericytes, arachnoid barrier cells (ABC), oligodendrocyte precursor cells (OPC), and olfactory ensheathing glia (OEG)). Each panel displays the distribution and magnitude of expression differences for the indicated mtDNA gene. Pairwise comparisons between mKate2+ and mKate2- cells were performed within each cell type using the two-sided Wilcoxon rank-sum text, with significance levels indicated as ns (not significant), *p < 0.05, **p < 0.01, ***p < 0.001, and ****p < 0.0001. Source data are provided as a Source Data file.

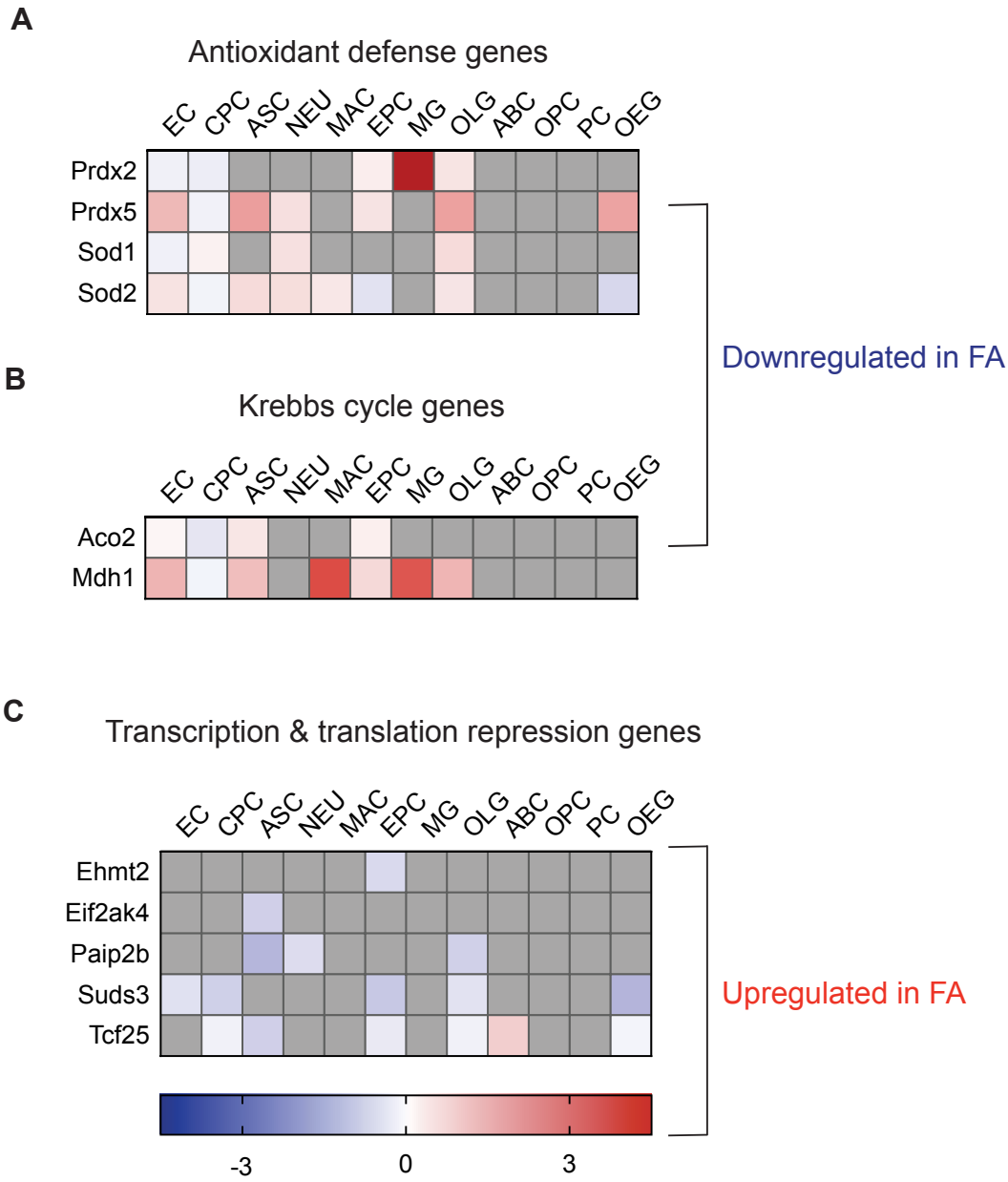

Supplementary Figure 13. Expression of antioxidant defense, Krebs cycle, and transcriptional repression genes in mKate2+ cells ccross CNS cell types. (A) Heatmap of antioxidant defense genes (*Prdx2, Prdx5, Sod1, and Sod2*) across various CNS cell types, including endothelial cells (EC), choroid plexus epithelial cells (CPC), astrocytes (ASC), neurons (NEU), macrophages (MAC), ependymal cells (EPC), microglia (MG), oligodendrocytes (OLG), arachnoid barrier cells (ABC), oligodendrocyte precursor cells (OPC), pericytes (PC), and olfactory ensheathing glia (OEG). These genes are typically downregulated in FA but show upregulation in mKate2+ cells, suggesting a recovery in antioxidant defense capacity. (B) Heatmap of Krebs cycle genes (*Aco2 and Mdh1*) across CNS cell types. These genes are usually downregulated in FA but are upregulated in mKate2+ cells, indicating potential restoration of metabolic function in these cells. (C) Heatmap of genes associated with transcriptional and translational repression (*Ehmt2, Eif2ak4, Paip2b, Suds3, and Tcf25*). These genes are typically upregulated in FA but show downregulation in mKate2+ cells, suggesting a reversal of transcriptional repression in certain cell types.The color scale represents relative expression changes, with shades of red indicating upregulation, shades of blue indicating downregulation, and gray representing non-significant data. Differential expression was assessed with the two-sided MAST test with Benjamini–Hochberg FDR correction (adjusted $p < 0.05$, fold change > 20%). Source data are provided as a Source Data file.

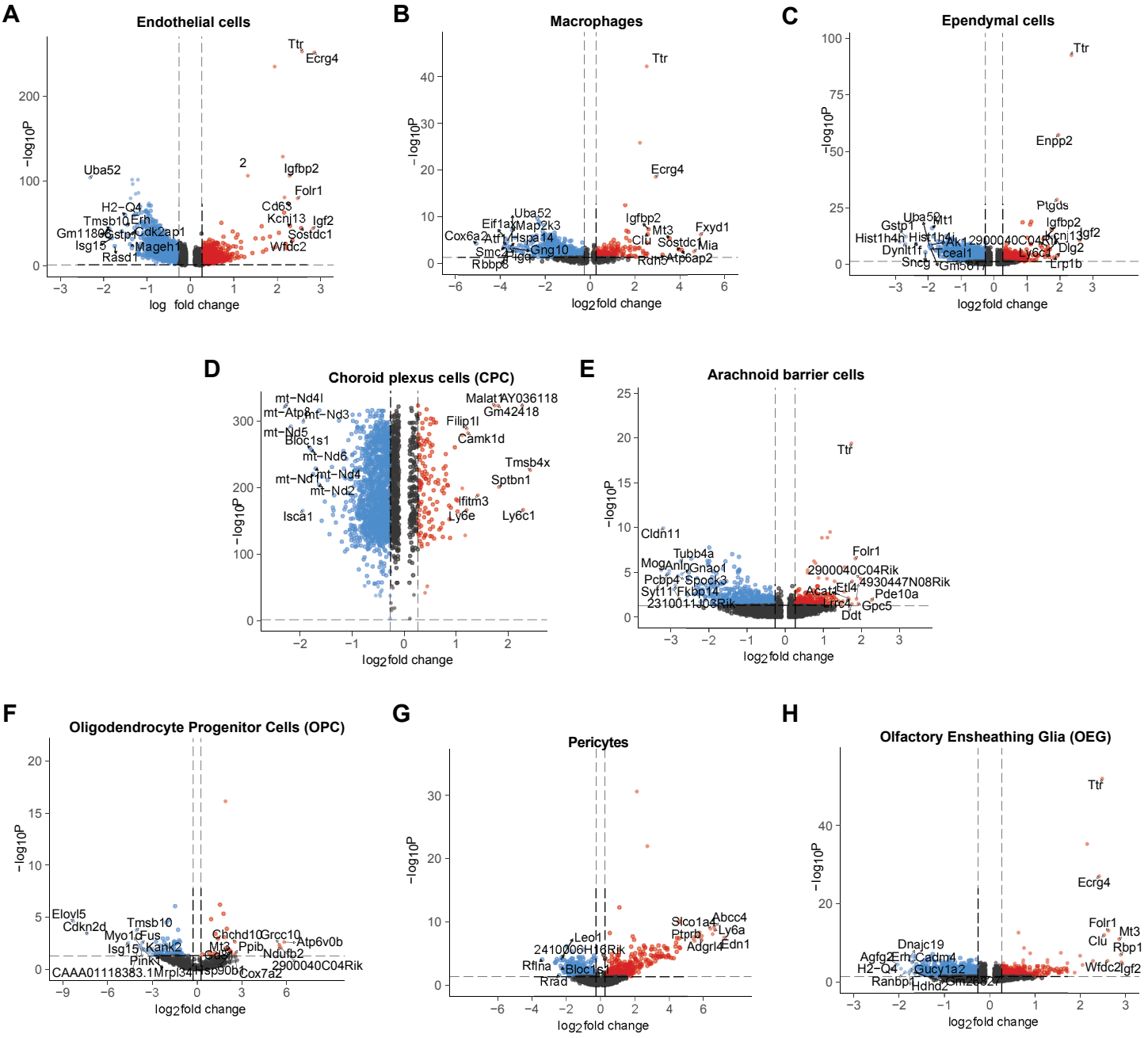

Supplementary Figure 14. Differentially expressed genes in mKate2+ and mKate2– CNS cell types following mitochondrial uptake. (A–H) Volcano plots showing differentially expressed genes between mKate2+ and mKate2- FA cells in (**A**) endothelial cells, (**B**) macrophages, (**C**) ependymal cells, (**D**) choroid plexus cells, (**E**) arachnoid barrier cells, (**F**) oligodendrocyte progenitor cells, (**G**) pericytes, and (**H**) olfactory ensheathing glia. Differentially expressed genes (DEGs) were identified using the two-sided MAST test with Benjamini–Hochberg FDR correction, considering genes that were expressed in at least 25% in either population). Blue dots show significantly downregulated genes (FC < -20%, p < 0.05), red dots show significantly upregulated genes (FC > 20%, p < 0.05), and genes represented by gray dots are not differentially expressed. The top upregulated and downregulated genes (by magnitude of log2 FC) are labeled.

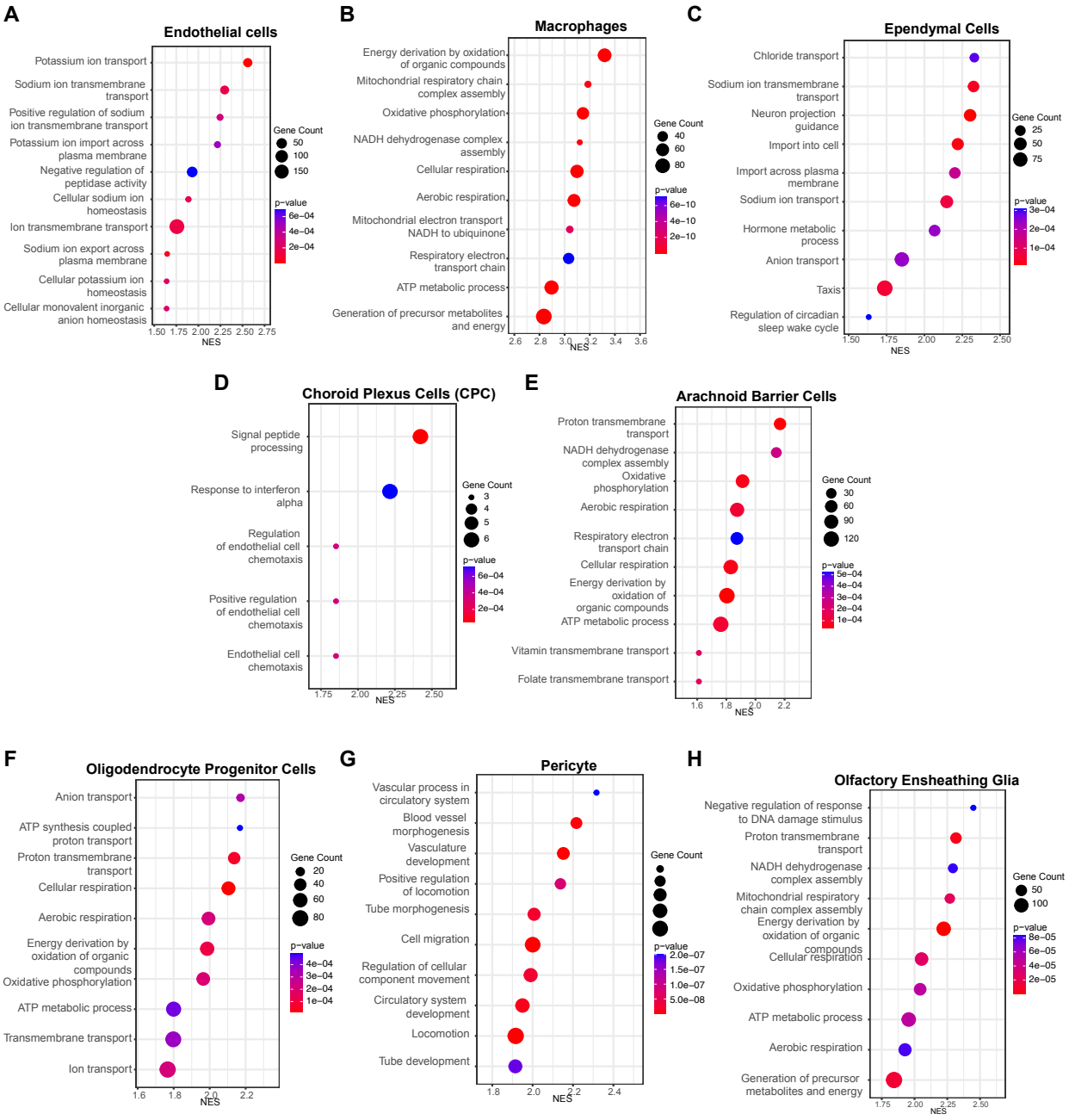

Supplementary Figure 15. Enriched pathways across CNS cell types following mitochondrial uptake. (**A-H**) Bubble plots showing the top 10 enriched gene sets by normalized enrichment score (NES) between mKate2+ and mKate2- FA cells in (**A**) endothelial cells, (**B**) macrophages, (**C**) ependymal cells, (**D**) choroid plexus cells, (**E**) arachnoid barrier cells, (**F**) oligodendrocyte progenitor cells, (**G**) pericytes, and (**H**) olfactory ensheathing glia. Gene sets are ordered by their NES, which reflects the extent to which each gene set is overrepresented at either the top or bottom of the ranked gene list, after normalizing for gene set size and score distribution in random samples. Each cell type's ranked gene list is created by ordering genes based on their average log2 fold change values, with the most positive values at the top and the most negative values at the bottom. The gene count indicates how many genes in each set are differentially regulated in our dataset. Enrichment was assessed by two-sided fGSEA against Gene Ontology Biological Process gene sets (significance $p < 0.05$, Benjamini–Hochberg $q < 0.25$). Data are from single-cell RNA sequencing of 12,347 GFP− recipient cells pooled from three biologically independent DP+FA mice.

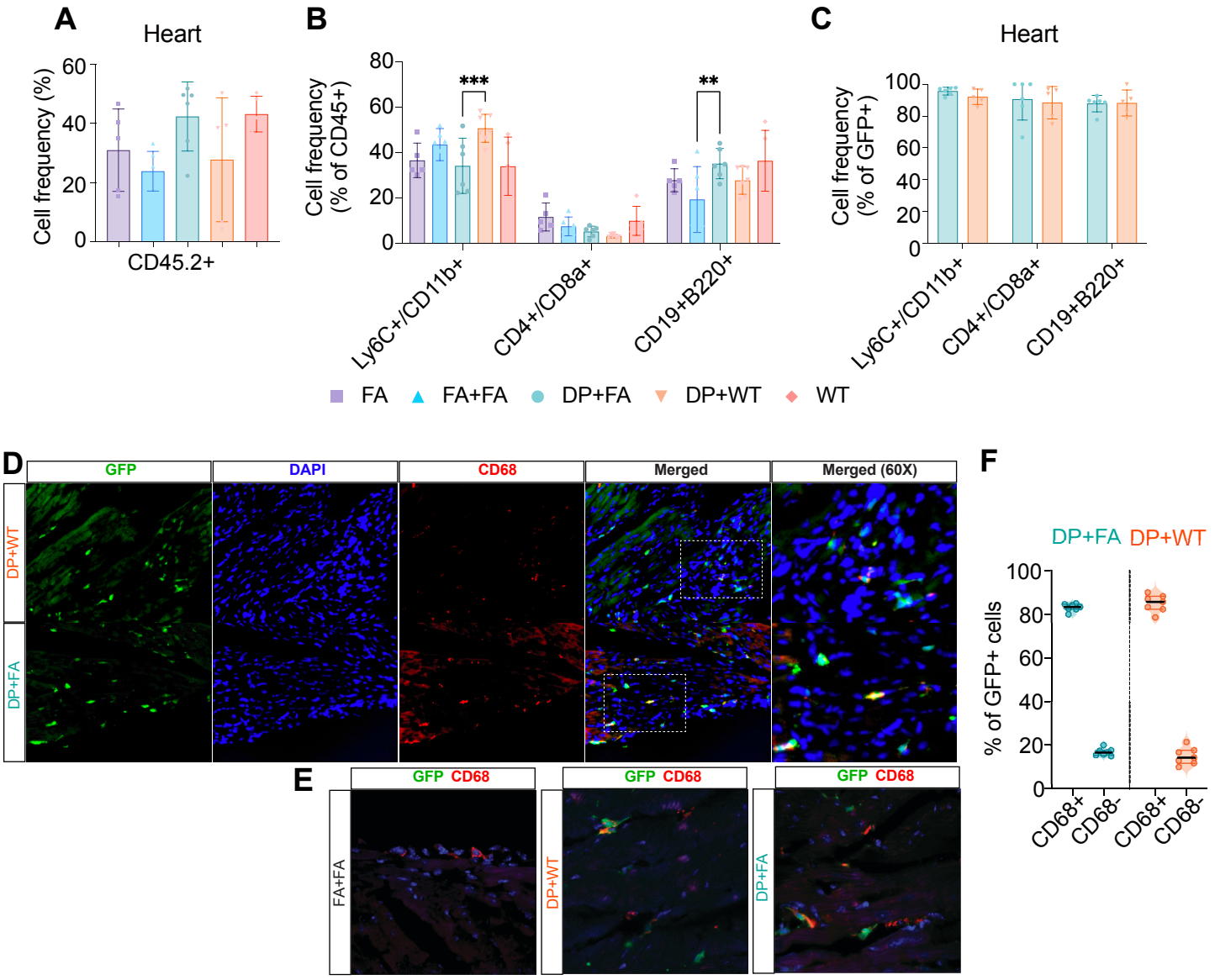

Supplementary Figure 16. Immune cell composition in heart following macrophage replacement. (A–C) Flow cytometric analysis of hematopoietic (CD45) cells in the heart five months post-transplantation. **(A)** Frequency of CD45 cells among live cells after isolation across experimental groups (WT, DP+WT, DP+FA, FA+FA). **(B)** Proportional distribution of CD45 subsets expressing CD11b/Ly6C (myeloid), CD19/B220 (B cell), and CD4/CD8a (T cell) markers. **(C)** Marker distribution among GFP cells. **(D)** Representative immunofluorescence images of cardiac tissue from the subendocardial regions of FA+FA, DP+FA, and DP+WT mice stained for GFP (green), CD68 (red), and DAPI (blue). **(E)** Representative confocal microscopy images of CD68/GFP cells with macrophage morphology. **(F)** Quantification of cardiac GFP cells shows the proportion of CD68 and CD68– cells in DP+FA and DP+WT groups. Data are presented as mean ± SD. Scale bars: 100 μm (low magnification), 20 μm (high magnification). Quantification was performed on ≥3 sections per mouse and ≥3 fields per section. All data are presented as mean ± SD. Each symbol represents one biologically independent mouse $n = 5$ per group. Statistical analysis for A was a two-sided Ordinary one-way ANOVA with Tukey multiple comparisons testing; for B and C, a two-sided Two-way ANOVA with Tukey multiple comparisons testing. Significant differences are indicated as $^{**}p < 0.01$ and $^{***}p < 0.001$. Exact p-values are provided in the Source Data file. Images in (D, E) are representative of $n = 5$ mice per group with similar results. Scale bars: 100 μm (low magnification), 20 μm (high magnification). Source data are provided as a Source Data file.

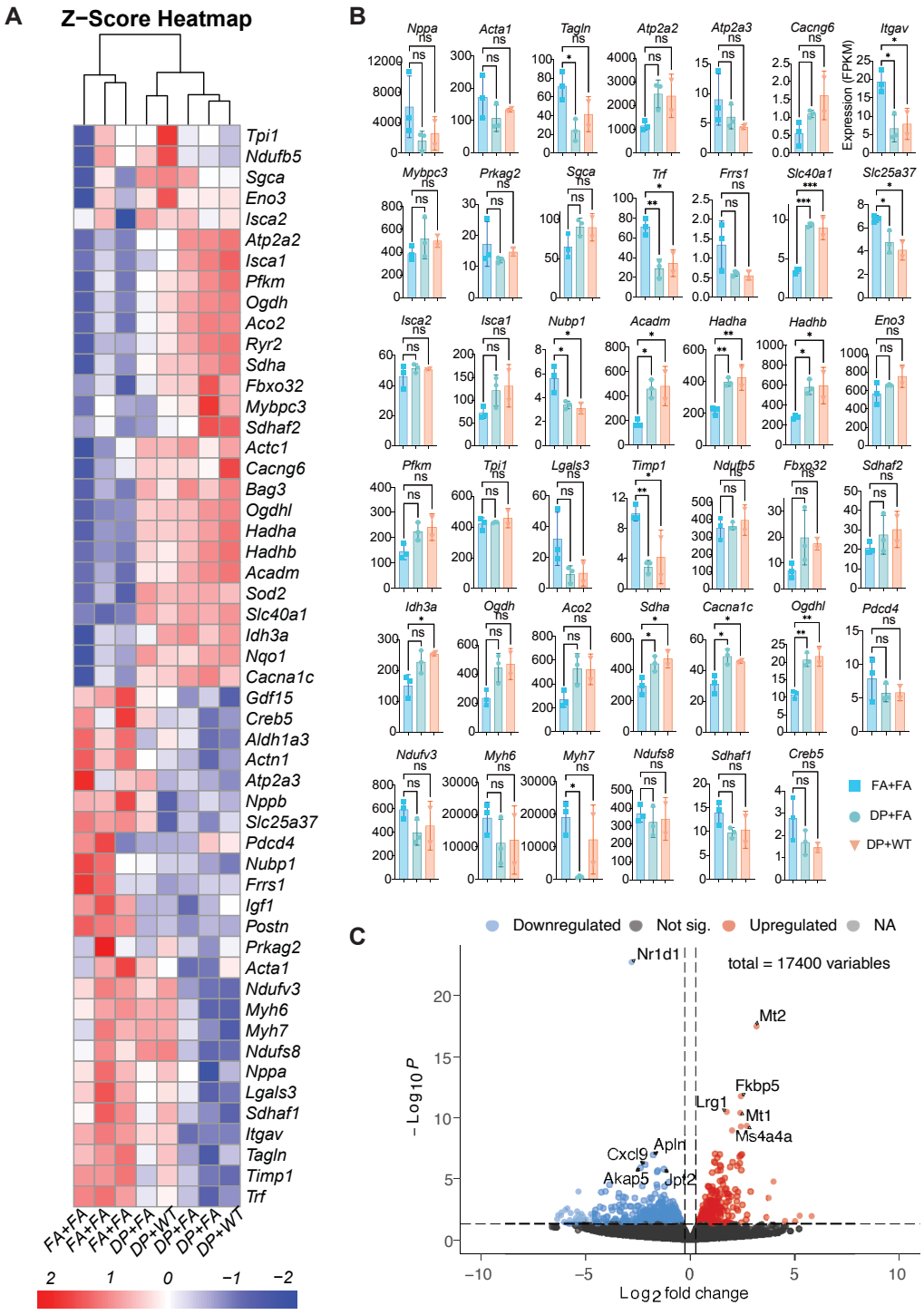

Supplementary Figure 17. Analysis of 52 markers genes associated with cardiac disease in FA mice and cell models. (A) Heatmap of Z-scores of FPKM expression values for the 52 marker genes across 8 samples (FA+FA, *n*=3; DP+FA, *n*=3; and DP+WT, *n*=2). Columns are ordered based on hierarchical clustering using complete linkage and Euclidean distance. The color scale indicates relative expression levels (red = up and blue = down). **(B)** Bar plots showing the gene expression (FPKM) levels for the remaining 41 genes, excluding the 12 genes presented in Figure 7H. Each symbol represents one biologically independent mouse (FA+FA, *n* = 3; DP+FA, *n* = 3; DP+WT, *n* = 2)**.** Statistical analysis was performed using one-way ANOVA with Sidak's multiple comparisons test compared to FA+FA (*p < 0.05; **p < 0.01; ***p < 0.001). Exact p-values are provided in the Source Data file. **(C)** Volcano plots showing differentially expressed genes between FA+FA and DP+FA hearts, identified by DESeq2. (n=3 for each sample). Blue dots show significantly downregulated genes (FC < -20%, p < 0.05), red dots show significantly upregulated genes (FC > 20%, p < 0.05), and genes represented by gray dots are not differentially expressed. The top five upregulated and downregulated genes, ranked by the magnitude of their -Log10 p-values, are labeled.

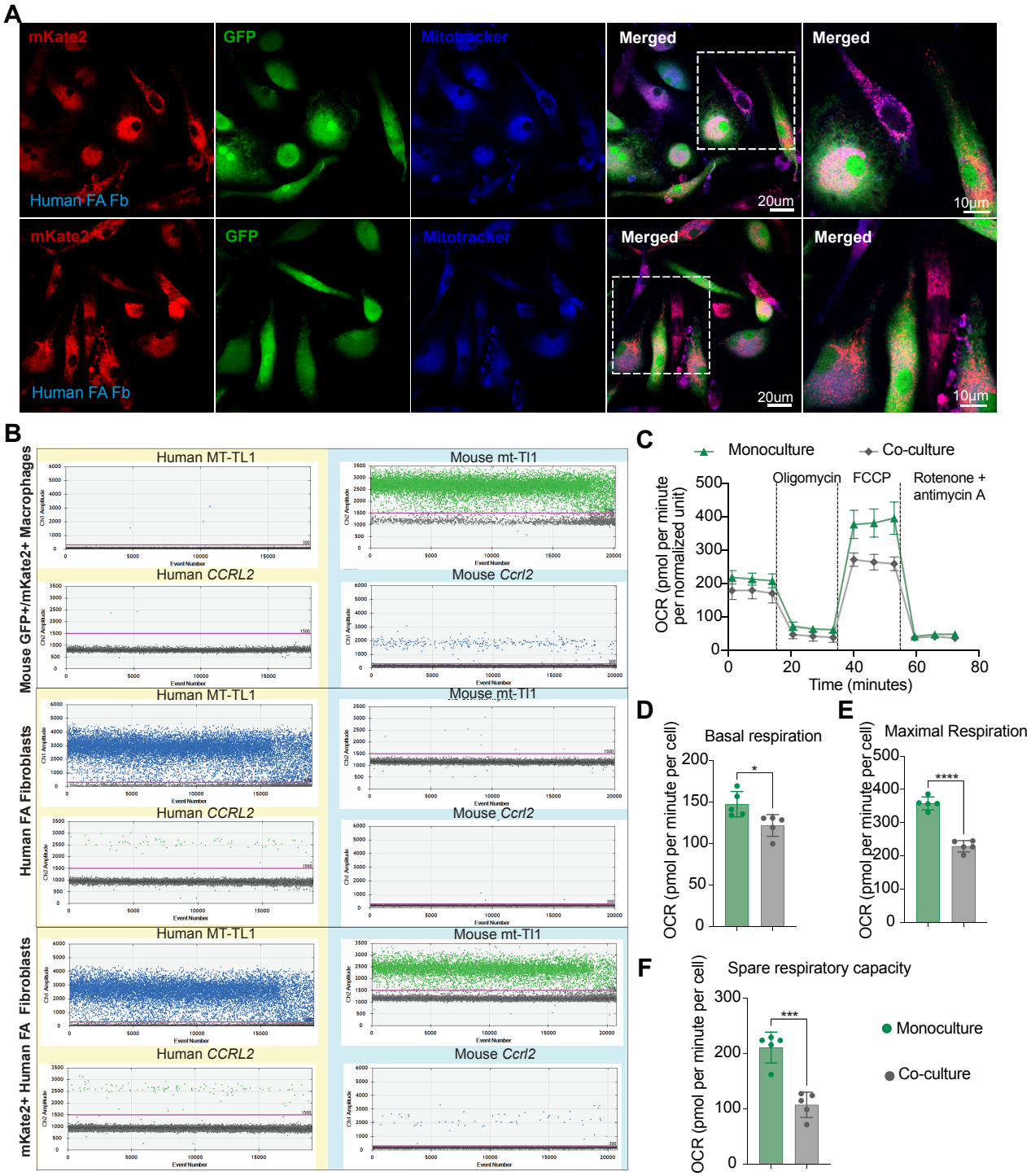

Supplementary Figure 18. Mitochondrial transfer in the macrophage–FA fibroblast axis. (A) Representative confocal images of human FA fibroblasts co-cultured with mouse GFP+/mKate2+ macrophages. Donor macrophages contain GFP-labeled cytoplasm (green) and mKate2-labeled mitochondria (red). Acceptor FA fibroblasts show mKate2+ signal colocalizing with MitoTracker (blue). Insets show high-magnification merged images. Scale bars: 20 μm (left insets), 10 μm (right insets). Images are representative of *n* = 3 independent experiments with similar results. **(B)** Representative ddPCR plots showing amplification of human and mouse mitochondrial (MT-TL1, mt-TI1) and nuclear (CCRL2, Ccrl2) genes in isolated GFP+/mKate2+ mouse macrophages (top), isolated human FA fibroblasts (middle), and mKate2+ human FA fibroblasts after direct co-culture with mouse macrophages. Plots are representative of *n* = 3 independent experiments. **(C)** Oxygen consumption rate (OCR) traces of mouse GFP+/mKate2+ macrophages cultured alone (monoculture) or with mouse FA fibroblasts (co-culture) following sequential addition of oligomycin, FCCP, and rotenone/antimycin A. **(D–F)** Quantification of basal respiration **(D)**, maximal respiration **(E)**, and spare respiratory capacity **(F)** in co-cultured vs. monocultured macrophages. Data are mean ± SD (each symbol represents one independent biological replicate; *n* = 5 independent experiments); comparisons were two-sided unpaired t test; *p < 0.05, **p < 0.01, ***p < 0.001, ****p < 0.0001. Exact p-values are provided in the Source Data file.

Species-specific ddPCR quantification of nuclear and mitochondrial DNA				
Probes				
Probe name	**Target species**	**Genome type**	**Sequence**	
Hs_MT-TL1	H. sapiens	Mitochondrial	56-FAM/TGGCAGAGC/ZEN/ CCGGTAATCGCA/3IABkFQ	
Mm_mt-Tl1	M. musculus	Mitochondrial	5HEX/ACAACCATT/ZEN/TGCAGACGCCA/ 3IABkFQ	
Hs_CCRL2	H. sapiens	Genomic	5HEX/AATTACACG/ZEN/ CTGGCACCAGAGGAT/3IABkFQ	
Mm_Ccrl2	M. musculus	Genomic	56-FAM/CTCTGCGGC/ZEN/ TGACAGAAGCT/3IABkFQ	
Primers				
Primer name	**Target species**	**Genome type**	**Sequence**	**Amplicon length (bp)**
Hs_MT-TL1_F	H. sapiens	Mitochondrial	CCCAAGAACAGGGTTTGT	75
Hs_MT-TL1_R	H. sapiens	Mitochondrial	TGAACCTCTGACTGTAAA GT	75
Mm_mt-Tl1_F	M. musculus	Mitochondrial	ACATACAACTACGAAAAG GC	100
Mm_mt-Tl1_R	M. musculus	Mitochondrial	GGGCGTATTGGTTCTTTT AT	100
Hs_CCRL2_F	H. sapiens	Genomic	CATCTCCCATTTCTCCAC AGG	98
Hs_CCRL2_R	H. sapiens	Genomic	GCTCTCCAGTTCACCTTC TATG	98
Mm_Ccrl2_F	M. musculus	Genomic	CTGGCTAAGAGGTACAG	113
Mm_Ccrl2_R	M. musculus	Genomic	GTTCTGAAAGCCTCTCTC	113

Supplementary Table 1. Species-specific ddPCR quantification of nuclear and mitochondrial DNA. Probe and primer sets used for droplet digital PCR (ddPCR) quantification of human nuclear genomic DNA (*CCRL2*), mouse nuclear genomic DNA (*Ccrl2*), and mitochondrial DNA (*MT-TL1* / m*t-Ll1*), featuring species-specific assays for *Homo sapiens* and *Mus musculus*.